Article

Not peer-reviewed version

A Modular Customizable Ligand-Conjugate (LC) System Targeting Ghrelin O-Acyltransferase

Amber L. Ford , Caine W. Taft , Andrea M. Sprague-Getsy , Gracie C. Carlson , Nilamber A. Mate , Michelle A. Sieburg , John D. Chisholm , James L. Hougland *

Posted Date: 4 December 2024

doi: 10.20944/preprints202412.0414.v1

Keywords: ghrelin; ghrelin O-acyltransferase; membrane-bound O-acyltransferase; GHSR, post translational modification; membrane enzyme, protein acylation, peptide mimetic inhibitor

 doi:10.20944/preprints202412.0414.v1

Article

A Modular Customizable Ligand-Conjugate (LC) System Targeting Ghrelin *O*-Acyltransferase

Amber L. Ford [1], Caine W. Taft [1], Andrea M. Sprague-Getsy [1], Gracie C. Carlson [1], Nilamber A. Mate [1], Michelle A. Sieburg [1], John D. Chisholm [1,2], and James L. Hougland [1,2,3,*]

[1] Department of Chemistry, Syracuse University, Syracuse, NY 13244, USA
[2] BioInspired Syracuse, Syracuse University, Syracuse, NY 13244, USA
[3] Department of Biology, Syracuse University, Syracuse, NY 13244, USA
* Correspondence: Hougland@syr.edu; Tel.: 315-443-1134

Abstract: Ghrelin is a 28 amino acid peptide hormone that impacts a wide range of biological processes including appetite regulation, glucose metabolism, growth hormone regulation, and cognitive function. To bind and activate its cognate receptor, ghrelin must be acylated on a serine residue in a post-translational modification performed by ghrelin O-acyltransferase (GOAT). GOAT is a membrane bound O-acyltransferase (MBOAT) responsible for catalysis of the addition of an octanoyl fatty acid to the third serine of desacyl ghrelin. Beyond its canonical role for ghrelin maturation in endocrine cells within the stomach, GOAT was recently reported to be overexpressed in prostate cancer (PCa) cells and detected at increased levels in the serum and urine of PCa patients. This suggests GOAT can serve as a potential route for detection and therapeutic targeting for PCa and other diseases which exhibit GOAT overexpression. Building upon a ghrelin mimetic peptide with nanomolar affinity for GOAT, we developed an antibody conjugate-inspired system for customizable ligand-conjugate (LCs) synthesis allowing for attachment of a wide range of cargos. The developed synthetic scheme allows for facile synthesis of desired LCs and demonstrates our ligand system tolerates an extensive palette of cargos while maintaining nanomolar affinity against GOAT.

Keywords: ghrelin; ghrelin *O*-acyltransferase; membrane-bound O-acyltransferase; GHSR, post translational modification; membrane enzyme, protein acylation, peptide mimetic inhibitor

1. Introduction

Ghrelin is a 28 amino acid peptide hormone first discovered by Kojima and coworkers in 1999 [1]. Ghrelin was first coined as "the hunger hormone" due to its role in appetite stimulation [2–4], but has also been shown to play a role in a variety of important processes including growth hormone secretion and glucose metabolism [1, 5–7], stress response [8–10], learning and memory [11,12], and a potential role in eating disorders and addiction [13–23]. Its importance in these metabolic and physiological pathways makes ghrelin an attractive focus for potential therapeutic avenues for associated diseases.

Ghrelin exists in two forms in circulation: an activated form that is acylated with an oactanoyl moiety of fatty acid linked to the third serine (herby called ghrelin), and the deactivated form that has a free hydroxyl at the third serine (desacyl-ghrelin) [1,24,25]. Upon octanoylation, ghrelin binds its cognate receptor, the growth hormone secretagogue receptor (GHSR) [26–28]. GHSR is a G-protein coupled receptor (GPCR) that, when activated by ghrelin, initiates several signaling cascades [7,29]. The unique covalent addition of the octanoyl chain to ghrelin is catalyzed by the enzyme ghrelin O-acyltransferase (GOAT) [30–32]. GOAT was originally discovered in stomach tissue [1]; however several studies have reported GOAT expression in a variety of tissues [31,33]. Notably, recent studies have reported the overexpression of GOAT in several cancers including prostate cancer and breast cancers [34–38]. These cancer cells are also reported to express ghrelin which may be acting within a noncanonical pathway in these cells [37,39–43]. Furthermore, there is evidence supporting GOAT

 doi:10.20944/preprints202412.0414.v1

expression at the plasma membrane and in extracellular vesicles which expands upon its canonical localization in the endoplasmic reticulum [44–48]. Since GOAT is found overexpressed in some cancerous tissues [34,37], this makes GOAT an attractive target for potential diagnostic and therapeutic development.

To detect GOAT in biological systems, we developed a ghrelin-mimetic peptide ligand with high affinity and specificity for GOAT without off target binding to GHSR. Conjugating a fluorophore to this peptide ligand had minimal effect on GOAT affinity [44,49]. This success in adding cargo to the original ligand inspired further exploration of ligand conjugation to develop a ligand-conjugate (LC) system targeting GOAT. LC systems can provide an economical alternative approach to antibody-drug conjugates (ADCs) currently being explored as anticancer agents [50–53]. ADCs can provide cancer-specific treatment with a large therapeutic payload and minimal side effects [54]. These drugs have been shown in prostate cancer patients and in clinical trials to be effective as diagnostics and treatments [55–58]. While customizable and effective in treating cancer, ADCs are also expensive and difficult to synthesize [54]. Due to the rigor required to synthesize ADCs and lack of ADCs for prostate cancer, we propose using a peptide-based approach to targeting GOAT to develop new cancer diagnostics or therapeutics. This approach may mitigate the expense and difficulty associated with synthesizing ADCs, replacing them with a lower cost system.

Towards this goal, we have developed a customizable system for developing GOAT-targeted ligand conjugates (LCs) using a parent peptide sequence with high affinity and specificity for GOAT, a novel bifunctional linker molecule, and an array of cargo molecules. Using this modular synthetic scheme, we developed of a library of GOAT specific ligands with different cargoes. Ligand characterization demonstrated a broad tolerance to cargo attachment without loss of binding affinity to GOAT, although linker composition can negatively impact ligand potency. This customizable system for generating potent GOAT-specific ligands may be used in the future for prostate cancer detection and treatment.

2. Materials and Methods

2.1. General

All parent peptides (3, 3', 4, 16, and 16') were commercially available by BioBasic (Markham, Ontario, Canada) and Pepmic (Suzhou, China). Peptides were solubilized in 50% aqueous acetonitrile and ultrapure water at 5 mM (by peptide mass) for testing and storage at -20°C. Following synthesis, the bifunctional adapter was solubilized in 50% aqueous acetonitrile at 20 mM and aliquoted for storage at -20°C. TAMRA azide was purchased from Click Chemistry Tools (Scottsdale, AZ) and solubilized at 10 mM concentration in 500 μL of DMSO for storage while protected from light at -20°C. Fluorophores AF488 alkyne, AF488 azide, FAM5 azide, SulfoCy5 azide, and SulfoCy5 maleimide were obtained from Lumiprobe (Hunt Valley, Maryland) and solubilized in anhydrous DMSO in 10 mM stocks and stored at -20°C protected from light. Quenchers TideQuencher2, AzoDye1 alkyne, and AzoDye1 azide were obtained from AAT Bioquest (Pleasonton, California) and solubilized in anhydrous DMSO in 1 mM stocks and stored at -20°C protected from light. Mertansine was obtained from Cayman Chemical (Ann Arbor, MI) and was solubilized in DMSO in 20 mM aliquots stored at -20°C. Methyl arachidonyl fluorophosphonate (MAFP) was diluted in DMSO from a stock in methyl acetate obtained from Cayman Chemical (Ann Arbor, MI). Octanoyl coenzyme A (octanoyl CoA, free acid) was purchased from AdventBio (Elk Grove Village, Illinois) and was solubilized to 5mM in 10 mM Tris-HCL pH 7.0 and stored in low adhesion tubes at -80°C until use. The GSSFLCNH2 peptide used in fluorescent acrylodan labeling were obtained from Sigma-Genosys (The Woodlands, TX) and synthesized in Pepscreen format. The GSSFLCNH2 peptide was solubilized in 100% acetonitrile and stored at -80°C. Acrylodan was obtained from Fisher Scientific (Waltham, Massachusetts) and solubilized in 100% acetonitrile in 2.2 mM stocks for storage at -80°C and protected from light until use. Copper (I) iodide, copper (II) sulfate, and sodium ascorbate were obtained from Sigma Aldrich (Burlington, Massachusetts) and stored at room temperature. Tris(3-hydroxypropyltriazolylmethyl) amine (THPTA) was obtained from Lumiprobe (Hunt Valley,

 doi:10.20944/preprints202412.0414.v1

Maryland) and stored at -20°C protected from light. MALDI matrix α- Cyano- 4- hydroxycinnamic acid (HCCA, Sigma Aldrich, Darmstadt, Germany) was stored at room temperature. Stocks were created as indicated in the MALDI sample preparation section at stored at room temperature until use. Fresh stocks were created every 6 months.

2.2. Peptide Ligand Concentration Determination

Peptide ligand concentrations were determined by UV-Vis absorbance using various chromophores. For peptides lacking a fluorophore or quencher cargo, concentrations were determined using absorbance of the unnatural amino acid 1-naphthylalanine (Nal) at 280 nm (ε280= 3936.12 M-1 cm-1) [46,69]. Concentrations for ligands containing fluorophores were determined using fluorophore absorbance as follows: TAMRA, absorbance at 553 nm (λ_{ex}=553 nm, λ_{em}=575 nm, ε_{553}= 92,000 M^{-1} cm^{-1}, per manufacturer); FAM5, absorbance at 492 nm (λ_{ex}=492 nm, λ_{em}=517 nm, ε_{492}= 74,000 M^{-1} cm^{-1} per the manufacturer); AF488, absorbance at 495 nm (λ_{ex}=495 nm, λ_{em}=519 nm, ε_{495}= 71,800 M^{-1} cm^{-1}, per manufacturer); SulfoCy5, absorbance at 646 nm (λ_{ex}=646 nm, λ_{em}=662 nm, ε_{646}= 271, 000 M^{-1} cm^{-1}, per manufacturer). Concentrations for ligands containing quenchers were determined using quencher absorbance as follows: AzoDye1 azide, 522 nm (ε_{522}= 34,000 M^{-1} cm^{-1}), AzoDye1 alkyne, 522 nm (ε_{522}= 34,000 M^{-1} cm^{-1}), TideQuencher2 azide, 540 nm (ε_{540}= 21,000 M^{-1} cm^{-1}).

2.3. Bifunctional Adapter Synthesis

The bifunctional adapter was synthesized from the corresponding diol precursor in two steps. Details of synthetic protocols and compound characterizations are reported in the Supplementary Material.

2.4. hGOAT Channel Computational Analysis

The distance from the putative active site/ligand binding site to the surface of hGOAT were determined using the computational model of hGOAT, with distances analyzed using the PyMOL Molecular Graphics System, Version 2.5.3 Shrödinger, LLC. The average distance between the residue His338 and residues lining the luminal pore were measured using the wizard measurement tool. For the computational model of hGOAT, residues M1, E105, l232, and S401 were selected based on their proximity to the entrance of the transmembrane channel. The distance from His338, atom NE2 was calculated to atom SD on M1, atom CD on E105, atom CG on L232, and atom OG on S401. Images of model were all created within the PyMOL Molecular Graphics System, Version 2.5.3 Shrödinger, LLC.

2.5. Copper-Catalyzed Cycloaddition For Cargo Attachment

2.5.1. Cu(I)I Azide-Alkyne Cycloaddition

For the majority of the copper catalyzed cycloaddition of azidohomoalanine or azide-bearing cargoes and alkynes, a literature procedure was followed [70]. The standard protocol combined 3.3 mg (0.017 mmol) Cu(I)I and 7 mg (0.013) mmol TBTA in 500 μL 4:1 DMF:H2O in a 5 mL test tube equipped with a stir bar. The mixture was allowed to stir for approximately 15 minutes until the reaction turned a pale-yellow color. For conjugation of the parent AHA-peptide (azide) and bifunctional linker (alkyne), after mixing 0.0004 mmol (160 μL, 5 mM stock) of parent peptide was added along with 0.004 mmol (2.1 mg) of the bifunctional linker. For conjugation of the AHA-linker conjugate (alkyne) and TAMRA azide (azide), after mixing, 0.0004 mmol of parent peptide or peptide-linker conjugate were added along with 0.004 mmol of cargo, with volumes varying depending on concentration. This protocol was halved or doubled based on the amount of starting material available. The reaction was allowed to stir vigorously approximately 18 h at room temperature. The final reaction turned a dark brown-yellow color. The reaction was then transferred

 doi:10.20944/preprints202412.0414.v1

to a 1.5 mL Eppendorf tube and centrifuged at maximum speed for 10 minutes to prepare for HPLC purification as described below.

2.5.2. Cu(II)SO_4 Azide-Alkyne Cycloaddition

The protocol followed for this method of azide-alkyne cycloaddition was modeled after a reported protocol optimized by the manufacturer from BraodPharm [71]. 200 mM tris-hydroxypropyltriazolylmethylamine (THTPA), 100 mM copper sulfate pentahydrate ($CuSO_4$-5H2O), and 100 mM sodium ascorbate were prepared in UP H_2O prior to the reaction. The copper:THPTA complex was formed by creating a 1:1 mixture of THPTA and CuSO4-5H2O (1:2 ratio of CuSO4-5H2O:THPTA) and allowing it to incubate for 15 minutes until a dark blue color appeared. After complex formation, 37.5 µL of the complex (7.5 and 15 µM concentrations, respectively), 12 mM sodium ascorbate, 300 µM Dap-AHA, and 1.2 mM AF488 alkyne were combined in a black 1.5 mL Eppendorf tube and allowed to stand for 1 hour at room temperature. Semipreparative HPLC purification of the product was achieved using the method described in the next section.

2.6. Thiol-Maleimide Conjugation For Cargo Attachment

For thiol maleimide conjugations, 300 µM of peptide (parent or parent-linker conjugate) and 500 µM bifunctional linker or cargo (mertansine) were combined in 50 mM HEPES buffer pH 7.8 and 50% v/v acetonitrile in a total volume of 500 µL. Conjugation of the AHA-linker conjugate with mertansine required dropwise addition of mertansine to prevent disulfide formation. Conjugation reactions were vortexed for approximately 16 h at room temperature at mid-speed. Vortexing was achieved using a Vortex Genie 2 from Scientific Industries (Bohemia, NY). Reactions were purified by HPLC as described below.

2.7. Purification of LCs via Semipreparative HPLC

Peptide conjugation reactions were purified by semipreparative reverse-phase HPLC (Zorbax Eclipse XDB-C18 column, 9.4 x 250 mm) using a solvent gradient from 2% acetonitrile in 0.05% aqueous TFA to 98% acetonitrile in 0.05% aqueous TFA over 35 minutes at a flow rate of 4.2 mL/min, followed by 100% acetonitrile for 10 minutes. The total time for each run is 45 minutes. Peptides and conjugates were detected by UV absorbance at 280 nm by the unnatural amino acid 1-naphthylalanine, and peptides were collected in 1.5 mL Eppendorf tubes. Retention times of all LCs are reported in Supplemental Table S1. Chemstation for LC (Agilent Technologies) was used for peak integration to determine purity. All samples were dried by SpeedVac (Eppendorf Vacufuge plus, Enfield, CT) for 10 hours under vacuum. Dried peptides and LCs were redissolved in 30-60 µL of 50% aqueous acetonitrile. Concentrations were determined by UV-visible absorbance (ThermoFisher scientific nanodrop 2000c spectrophotometer) at the specified wavelength as described above. All stocks were stored at -20oC.

2.8. MALDI Characterization of LCs

LCs were characterized by MALDI mass spectrometry using an α-cyano- 4- hydroxycinnamic acid (CHCA, Sigma Aldrich, Darmstadt, Germany) matrix. Samples were analyzed by MALDI-TOF Microflex LRF (Bruker) using the RP 500-3500 Da method. MALDI spectra were analyzed by FlexAnalysis software. Masses for all LCs are reported in Supplementary Table S1.

2.9. IC_{50} Protocol

Microsomal fraction containing hGOAT for ligand binding studies by IC_{50} determination was prepared according to published protocols.67 For the GOAT inhibition assay, serial dilutions of 0, 0.15, 0.5, 1, 5, 15, and 50 µM concentrations were prepared in 50% acetonitrile for each ligand used. Membrane fractions from Sf9 cells expressing GOAT were first thawed on ice, then passed through an 18-gauge needle ten times to homogenize. Assays were performed with approximately 30 µg of membrane protein as determined through a Bradford assay. Standard reaction conditions contained

 doi:10.20944/preprints202412.0414.v1

50 mM HEPES pH 7.0, 1 μM MAFP, 30 μg of membrane protein, and ultra-pure water. Ligands were added to reaction mixtures and incubated for 30 minutes at room temperature protected from light prior to reaction initiation. Reactions were initiated by octanoyl CoA (300 μM final concentration) and $GSSFLC_{Acdan}$ (0.3 μM final concentration) in a total reaction volume of 50 μL. Reactions were incubated for 45-120 minutes protected from light at room temperature until 30-50% substrate acylation was observed in the vehicle control. Reactions were stopped with 50 μL of 20% acetic acid in isopropanol. Excess membrane fraction was precipitated with 16.7 μL of 40% trichloroacetic acid (TCA) followed by a 1000 x g centrifugation for 2 minutes. The supernatant was then analyzed via reverse-phase HPLC in 100 μL samples as previously described [67]. Inhibition trials were run in triplicate with the reported IC_{50} values representing the average of at least three trials.

2.10. Analysis of GOAT Inhibition Assays Via Analytical HPLC

Assays were analyzed on reverse-phase HPLC (Zorbax Eclipse XDB column, 4.6 x 150 mm) using a solvent gradient from 100% acetonitrile to 63% acetonitrile in aqueous 0.05% TFA over 5 minutes at a flow rate of 1 mL/min, followed by a gradient of 100% acetonitrile in 0.05% TFA to 63% acetonitrile in 0.05% TFA over 1 minute, 100% acetonitrile for 5 minutes, and a gradient of 100% acetonitrile to 30% acetonitrile in 0.05% TFA for 5 minutes. The total time for each run is 16 minutes. Peptides were detected by the attached acrylodan label with the UV absorbance at 360 nm and fluorescence (λ_{ex} = 360 nm, λ_{em} = 485 nm). Octanoylated peptide typically eluted around 7.5 minutes, with the unreacted peptide eluting around 2.5 minutes. Chemstation for LC (Agilent Technologies) was used for peak integration.

2.11. Determination of IC_{50} values

Peak integrations were used to determine percent conversion in the presence of either inhibitor (ligand, LDC) or vehicle (50% acetonitrile). Percent activity was calculated using equation 1:

$$\%\ \text{peptide octanoylationa} = \frac{\text{fluorescence of octanoylated peptide}}{\text{total peptide fluorescence}}, \quad (1)$$

IC_{50} values were determined by fitting equation 2 to the plot of % activity against inhibitor concentration. $\%\ \text{activity} = \%\ \text{vehicle}\left(1 - \frac{[\text{Inhibitor}]}{[\text{Inhibitor}]+IC50}\right)$ (2)

Plots and data fitting were performed with Kaleidagraph (Synergy Software, Reading, PA).

3. Results and Discussion

3.1. Design of Modular Ligand-Conjugate System

We previously reported development of a ghrelin mimetic ligand (**1**) with high specificity and affinity for GOAT based on structure-activity relationships, and further modification yielded the second-generation ligand with a fluorescent SulfoCy5 tag (**2**) (Figure 1a) [49]. Attachment of this fluorophore yield a small 3-fold loss of binding potency to GOAT. To reduce the likelihood of cargo interaction with GOAT in our ligand-conjugate library, we examined the structural model of human GOAT to determine the optimal ligand and linker lengths. In this analysis, we leveraged our finding that interaction between the Dap amino side chain at the third position of the peptide ligand and the conserved H338 residue within the GOAT catalytic channel is essential for ligand binding [44]. This catalytic channel, which is a common feature of protein-modifying MBOAT family members [59–62], connects the pore through which ghrelin enters the core of GOAT with the acyl donor binding site at the enzyme's cytoplasmic face [46]. The side chain of H338 lies ~21 Å from the pore interface, as measured to four GOAT residues on the pore periphery (Figure 1b). With five amino acids between the Dap residue contacting H338 and the fluorophore attachment point, this distance is compatible with the fluorophore in ligand **2** lying outside the GOAT channel and exposed to solvent [63,64]. However, in our customizable ligand-conjugate system we chose to add additional spacing between the GOAT ligand and the cargo to further reduce any chance for direct cargo contact with GOAT or its proximal membrane lipids.

 doi:10.20944/preprints202412.0414.v1

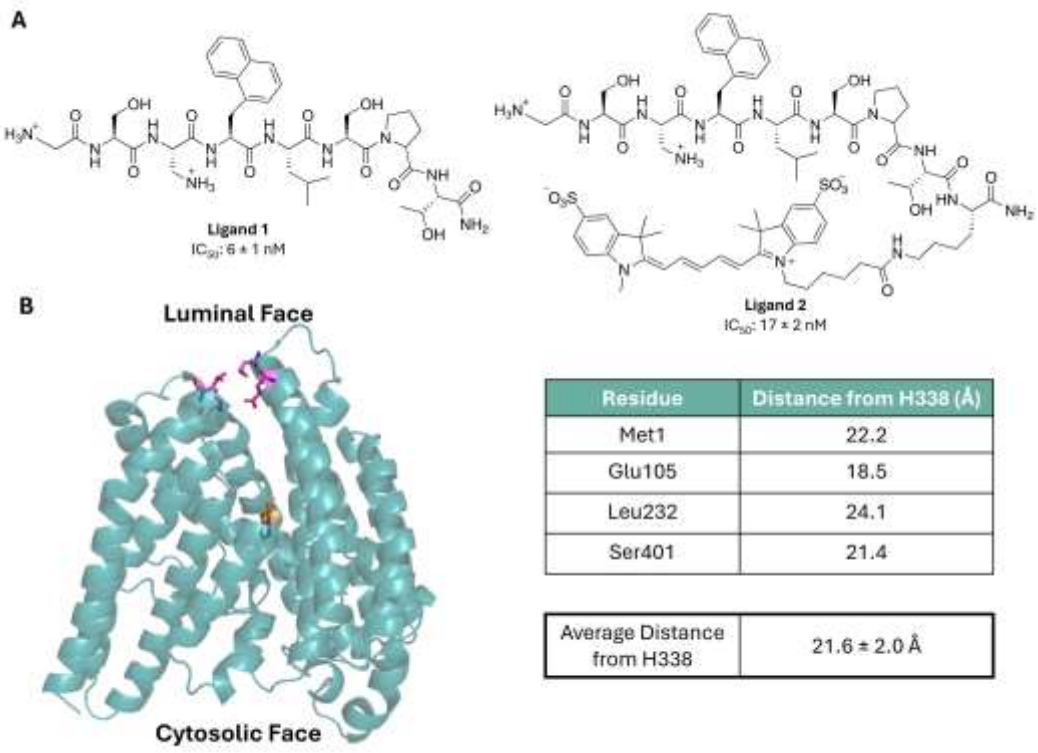

Residue	Distance from H338 (Å)
Met1	22.2
Glu105	18.5
Leu232	24.1
Ser401	21.4

Average Distance from H338	21.6 ± 2.0 Å

Figure 1. Initial ligands and constraints for a new generation of customizable GOAT ligands. A) Structures of GOAT ligand **1** and its fluorophore conjugated derivative ligand **2** [44]. B) Computational model of human GOAT (hGOAT) depicting distance from conserved catalytically essential H338 residue and multiple resides residing on the luminal pore through which ghrelin is proposed to enter the enzyme catalytic transmembrane channel. Distances for each pore residue are measured from the H338 side chain as described in the Material and Methods. hGOAT is shown in dark teal, H338 is shown in orange, and selected pore-defining residues (Met1, Glu105, Leu232, and Ser401) are shown in magenta. The hGOAT computational model was created in PyMOL Molecular Graphics System.

For the GOAT peptide ligand in this ligand-conjugate system, we designed two parent peptides predicted to maintain nanomolar affinity for GOAT while allowing for ample customization at their C-terminii. These peptides share the same eight reside ghrelin-mimetic sequence as the previously developed ligands followed by a mini-PEG3 linker terminating with either a C-amidated cysteine residue (**3**) for thiol-maleimide conjugation or C-amidated azidohomoalanine (**4**) for azide-alkyne copper catalyzed cycloaddition (Figure 2a). To provide for further spacing between the peptide ligand and the cargo and allow for additional conjugation flexibility, we developed a novel bifunctional linker molecule containing maleimide and alkyne sites for cargo attachment using thiol-maleimide or azide-alkyne conjugation chemistries (Figure 2b). This bifunctional linker was inspired by the bifunctional maleimide-NHS ester linker used in trastuzumab-emtansine which is an FDA-approved ADC for treatment of HER2-positive breast cancer [65]. Our scheme combines these modular components with the desired cargo molecules in a customizable method for LC development (Figure 2c).

Preprints.org (www.preprints.org) | NOT PEER-REVIEWED | Posted: 4 December 2024 doi:10.20944/preprints202412.0414.v1

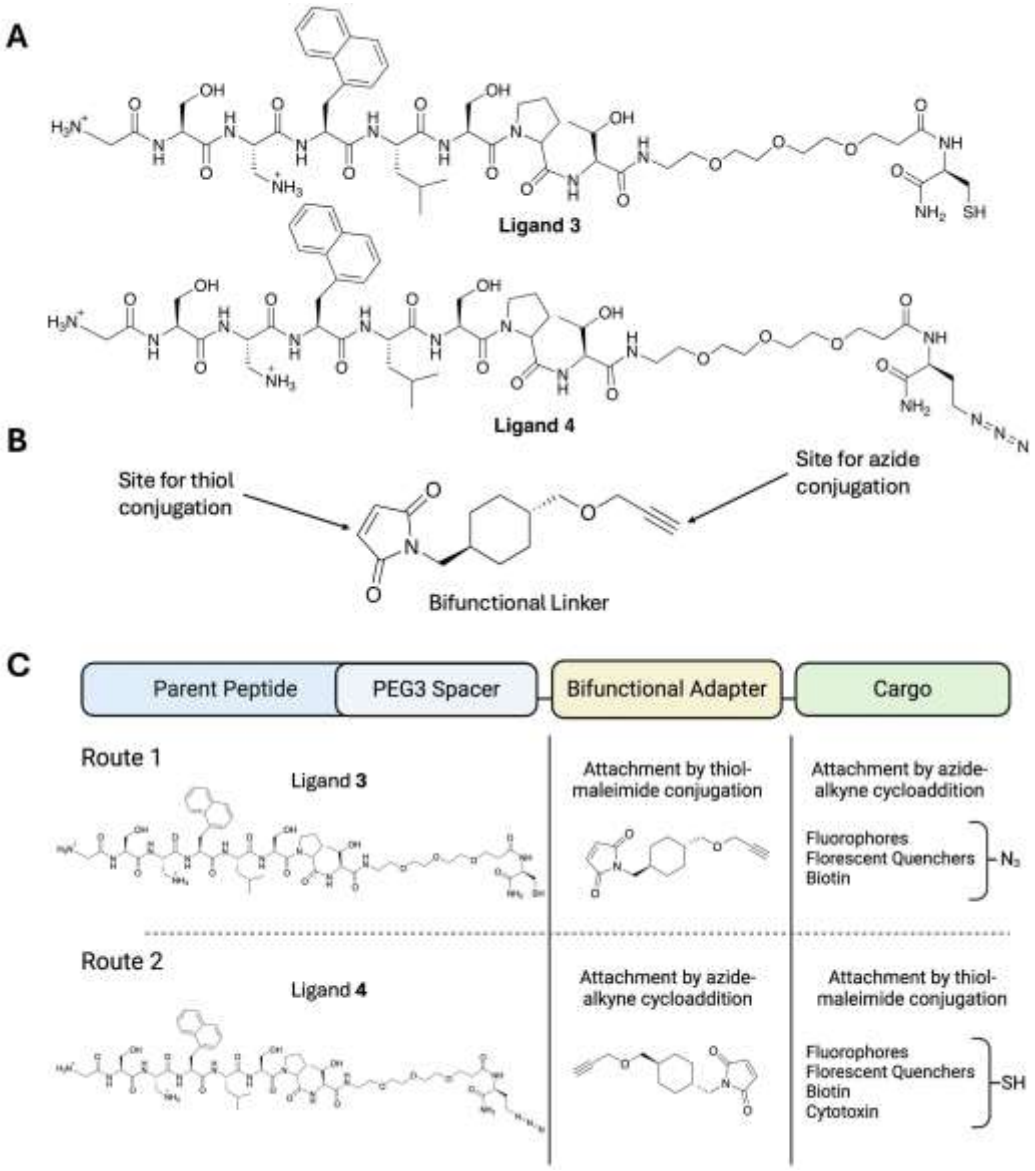

Figure 2. Design concept for GOAT ligand-conjugate (LC) system. A) Structures of parent ligands **3** and **4**, based on ligand **1** with PEG linker and chemospecific thiol or azide conjugation tags. B) Structure of bifunctional linker molecule. D) Scheme for construction of the customizable LC library including base ligand, PEG3 spacer, bifunctional adapter, and cargo. .

3.2. Ligand Synthesis and Characterization of GOAT Binding Potency

Binding potency to GOAT for all ligands and ligand conjugates was determined using our standard GOAT ghrelin acylation inhibition assay (Scheme 1) [66,67]. Both parent peptides **3** and **4** exhibited a five-fold decrease in GOAT affinity compared to first-generation ligand **1** and a two-fold decrease in GOAT affinity from the second-generation fluorescent ligand **2** but still maintained nanomolar affinity for GOAT (Figure 3a-b). These ligands can be used to directly attach to the cargo of choice using their thiol and azide moieties if rigidity or proximity to GOAT are warranted, or they can be further functionalized using the novel bifunctional linker molecule to introduce thiol- and azide-reactive attachment points. Ligand **3** was conjugated to the bifunctional linker using a thiol-maleimide addition to yield ligand **5**. Ligand **5** exhibits increased GOAT binding affinity with potency comparable to ligand **2** (Figures 1a and 3c). Attachment of the bifunctional linker molecule to parent ligand **4** was achieved using a copper-catalyzed azide-alkyne cycloaddition. This yielded ligand **6**, which exhibited in a drastic decrease in apparent GOAT inhibition potency (Figure 3d). This loss of potency may reflect sequestration of ligand **6** by reaction of the free maleimide thiol groups

 doi:10.20944/preprints202412.0414.v1

on background proteins in the membrane protein fractions used in our GOAT acylation assays [67]. If this maleimide side reactivity is the cause of the diminished binding for ligand **6**, we predict this effect with be alleviated by addition of thiol-bearing cargo to ligand **6** that will functionalize the maleimide group.

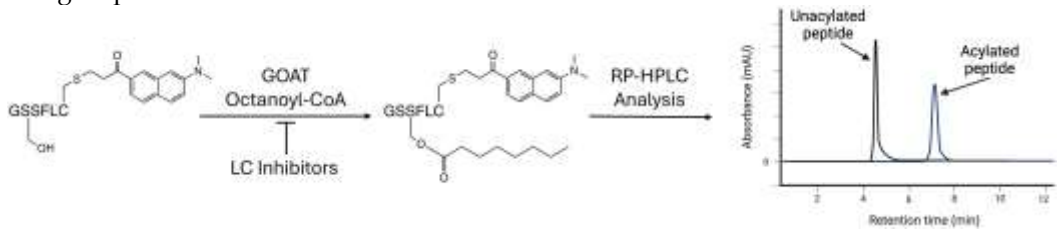

Scheme 1. GOAT inhibition assay for determining ligand binding. Octanoylation of a fluorescently-labeled ghrelin-mimetic peptide substrate is inhibited by LC binding, with GOAT octanoylation activity and inhibition determined as described in Materials and Methods.

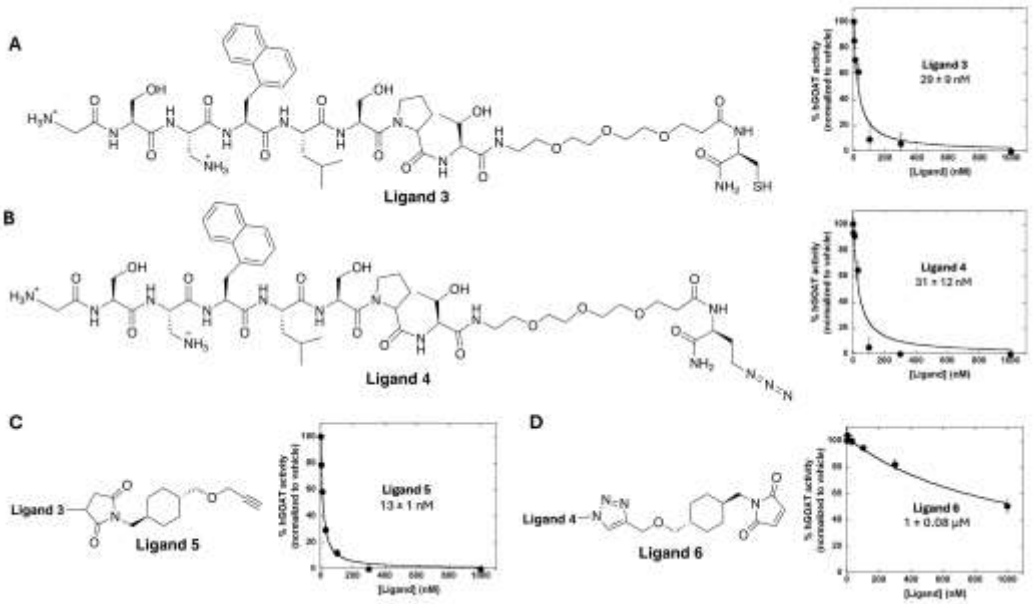

Figure 3. Parent ligand and ligand-linker conjugate binding to hGOAT. A) Structure and IC_{50} determination for Ligand **3** terminating in a cysteine residue. B) Structure and IC_{50} determination for Ligand **4** terminating in an azidohomoalanine (Aha) residue. C) Abbreviated structure and IC_{50} determination for Ligand **5**. D) Abbreviated structure and IC_{50} determination for Ligand **6**. IC_{50} values against hGOAT represent the average of three independent trials, and error bars represent one standard deviation.

3.3. Exploring Scope of Potential Cargo Molecules for GOAT Ligand Conjugates

Building upon ligand **5**, we determined the impact of cargo conjugation on GOAT binding potency. The first cargos explored were fluorophores to enable GOAT detection/labeling and ligand binding studies [44]. The fluorophores chosen covered a range of excitation and emission wavelengths as well as differing chemical properties (e.g. size and charge) to assess the diversity of cargo tolerated in this ligand-conjugate system. Fluorophore azides were conjugated to ligand **5** to create ligands **7** (AF488 azide), **8** (FAM5 azide), **9** (SulfoCy5 azide), and **10** (TAMRA azide). IC_{50} values for ligands **7**, **8**, and **9** are 6-8 fold higher than the parent ligand **5** with the AF488 ligand highest at ~100 nM (Figure 4a-c). Conversely, ligand **10** maintained the low IC_{50} value seen with ligand **5** supporting that attachment of cargo can result in little or no change to GOAT affinity (Figure 4d). The TAMRA fluorophore in ligand **11** has a positive charge which could contribute to maintaining high binding affinity. Notably, all fluorophore-conjugated ligands maintain sub-micromolar affinity well below the affinity for native ghrelin demonstrating the tolerance of our GOAT ligand-conjugate system for different cargoes [32,49].

 doi:10.20944/preprints202412.0414.v1

We also explored LCs functionalized with fluorescent quencher cargoes to be used in fluorescence resonance energy transfer (FRET) experiments, resulting in ligands **11** and **12** (Figure 4e-f). Ligand **11** bearing a TideQuencher2 cargo exhibited an IC_{50} approximately 2-fold higher than the parent ligand **5**. However, ligand **12** bearing an AzoDye1 cargo showed a drastic increase in GOAT binding potency to become the highest affinity GOAT-targeting peptide-based LC reported (Figure 4f). This increase in binding potency may be due to the linear nature of the AzoDye1 fluorescent quencher combined with the neutral charge and aromatic ring system of this cargo (Figure 4g). The AzoDye1 fluorescent quencher itself was tested for direct GOAT inhibition and showed no evidence for direct binding to the enzyme (data not shown).

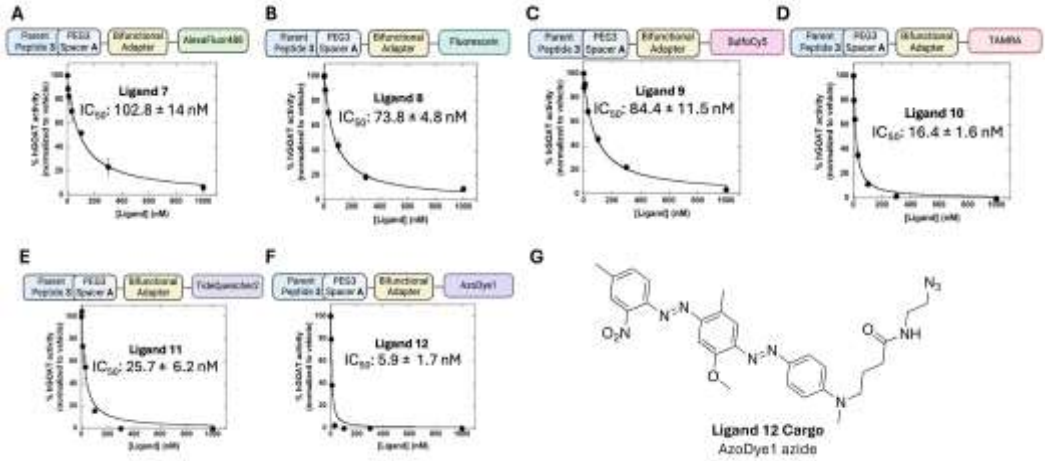

Figure 4. Assessment of cargo tolerance in hGOAT LC system. A-D) IC_{50} values for fluorescently conjugated ligands **7**, **8**, **9**, and **10** with AF488, fluoresceine, SulfoCy5, and TAMRA cargoes, respectively. E-F) IC_{50} values for ligands **11** and **12** with fluorescence quencher cargoes. G) Structure for the fluorescence quenching cargo AzoDye1 azide (ligand **12** cargo). IC_{50} values against hGOAT represent the average of three independent trials, and error bars represent one standard deviation.

Complementary to the fluorescent and quencher cargoes above, we found that attachment of cargoes for affinity labeling or potential therapeutic applications were similarly well tolerated by GOAT. Ligand **13** contains a biotin at the ligand C-terminal end to enable detection and isolation by streptavidin binding. This ligand did not include the bifunctional adapter and exhibited GOAT binding affinity within 2-fold of the comparable parent peptide ligand **3** (Figure 5a). Ligand **14** bears the cytotoxin mertansine attached to ligand **6** through thiol-maleimide conjugation, with this LC modeled after an FDA approved ADC cancer treatment for breast cancer (Figure 5b) [68]. Ligand **14** notably exhibits exceptional hGOAT binding affinity (~20 nM) compared to the >1 μM apparent IC_{50} observed with ligand **6**. This is consistent with our hypothesis that the aberrant ligand **6** potency was due to off-target reactions with thiols in the membrane protein fraction. Furthermore, the attachment of the large mertansine cargo without loss of binding potency further demonstrates the broad tolerance of our GOAT ligand conjugate system for a wide range of cargo molecules.

 doi:10.20944/preprints202412.0414.v1

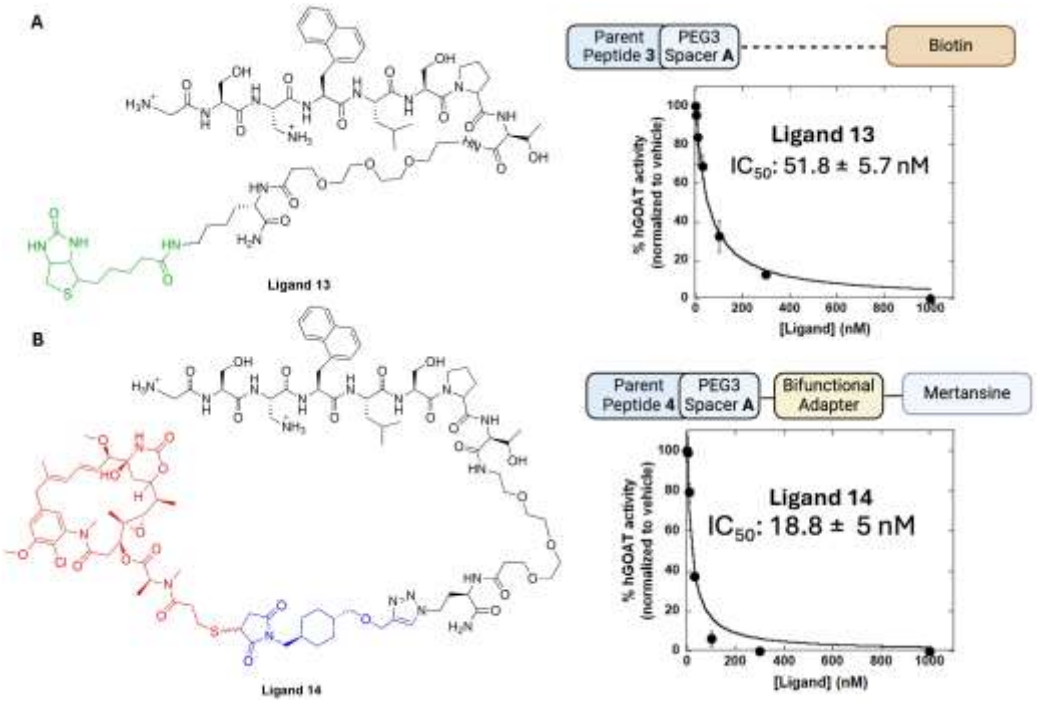

Figure 5. GOAT ligand-conjugates bearing affinity and cytotoxin cargoes effectively bind hGOAT. A) Ligand **13** containing a biotin cargo binds potently to hGOAT. B) Ligand **14** containing a mertansine cytotoxin cargo exhibits strong binding to hGOAT. IC_{50} values against hGOAT represent the average of three independent trials, and error bars represent one standard deviation.

3.4. Determining the Impact of Linker Groups on GOAT Ligand Conjugate Binding

Having established that our ligand conjugate system readily accepts a range of cargo molecules, we determined the importance of the two linker groups in our ligand design – the bifunctional adapter and the PEG3 linked connecting the core ghrelin ligand peptide to the C-terminal cysteine or azidohomoalanine residue. Attachment of the AF488, SulfoCy5, and AzoDye1 cargos directly to ligand **4** by azide-alkyne cycloaddition yielded ligands **15**, **16**, and **17**, respectively (Figure 6). In each case, the ligand without the bifunctional linker binds GOAT more tightly although this effect is less than 3-fold in all cases. This suggests the bifunctional adapter is not required to provide a rigid linker to separate the cargo from GOAT, but in future ligand development incorporation of the bifunctional adapter can be explored (particularly in the case of larger cargo molecules) without concern for substantial loss of binding potency to GOAT.

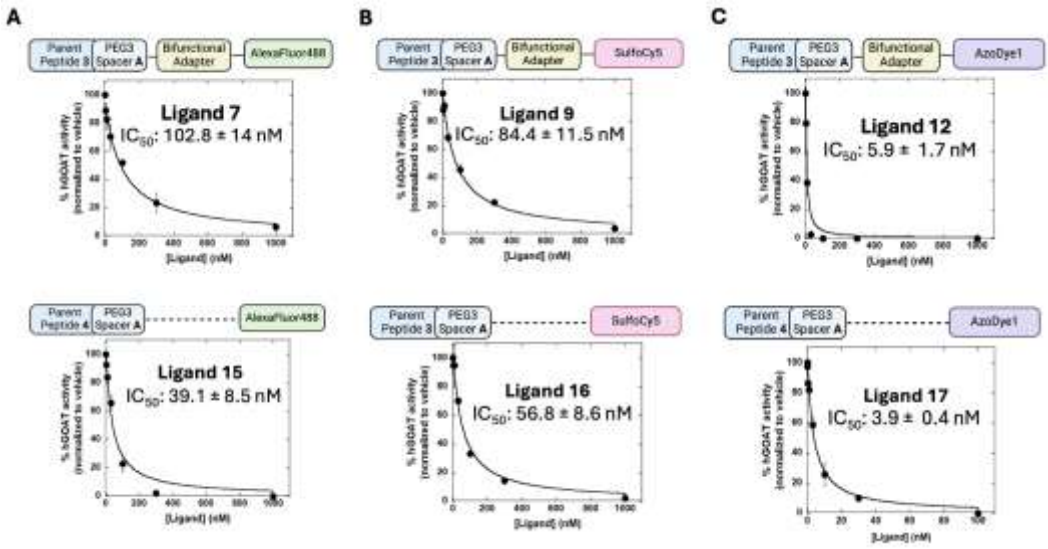

Preprints.org (www.preprints.org) | NOT PEER-REVIEWED | Posted: 4 December 2024 doi:10.20944/preprints202412.0414.v1

Figure 6. Determination of the impact of the bifunctional adapter molecule on hGOAT LC binding. The impact of the bifunctional adapter was determined by comparison of LCs bearing the same cargo with and without the adapter. A) AF488 fluorophore cargo; comparison of ligand **7** (with adapter) and ligand **15** (without adapter). B) SulfoCy5 fluorophore cargo; comparison of ligand **9** (with adapter) and ligand **16** (without adapter). C) AzoDye1 quencher cargo; comparison of ligand **12** (with adapter) and ligand **17** (without adapter). IC_{50} values against hGOAT represent the average of three independent trials, and error bars represent one standard deviation.

During preparation of our ligand conjugate library, we discovered the "mini-PEG3" linker offered by different commercial suppliers can vary in structure with either one or two methylene carbons between the carboxylate terminus and the first ether oxygen (Figure 7a). To determine if this change in linker structure could impact ligand binding to GOAT, we prepared ligands corresponding to ligands **3**, **13**, and **16** bearing the one-methylene version of the PEG3 linker (denoted linker B) (Figure 7b-d). In two of three cases, the incorporation of PEG3 linker B with the loss of a single methylene unit in the spacer resulted in a loss of binding potency with a ~4-fold drop for the parent peptide (**3** and **3'**) and a ~7-fold loss for the biotin-bearing ligand (**13** and **13'**). In contrast, the ligand bearing the Sulfo-Cy5 fluorophore with the PEG3 linker B exhibited a ~2-fold increase in binding affinity to GOAT compared to linker A (16 and **16'**). The decreased in IC_{50} value in this case may reflect specific properties of the sulfoCy5 fluorophore and interaction with either GOAT or the surrounding membrane phospholipids. SulfoCy5 is the only negatively charged cargo evaluated in this LC library, and notably the attachment of SulfoCy5 to each ligand in this study decreased GOAT binding affinity by at least 2-fold other than ligand **16'** with shortened PEG3 linker. These results highlight the structure of the mini-PEG3 linker as a potential variable to be considered in ligand design and optimization.

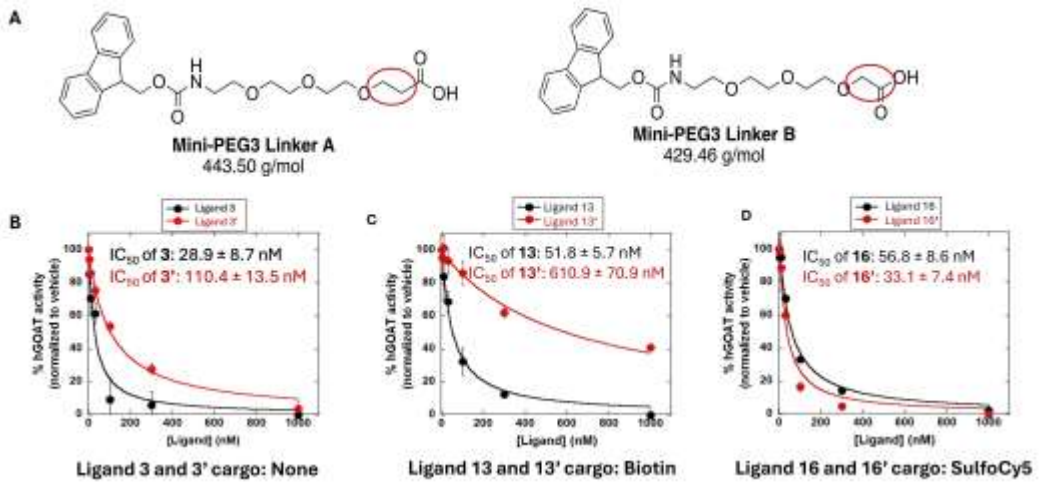

Figure 7. Mini-PEG3 linker composition can unexpectedly impact LC binding to hGOAT. A) Structures of mini-PEG3 linkers A (443.50 g/mol) and B (429.46 g/mol) used in commercially synthesized parent ligands and subsequently derived LCs. The linkers differ by a single methylene group (red oval) which lies proximal to the cysteine or AHA cargo conjugation site. LCs noted by a prime symbol indicate the presence of mini-PEG3 linker B. B) Overlay of IC_{50} curves for ligands **3** (mini-PEG3 linker A) and **3'** (mini-PEG3 linker B). C) Overlay of IC_{50} curves for ligands **13** (mini-PEG3 linker A) and 13' (mini-PEG3 linker B). D) Overlay of IC_{50} curves for ligands **16** (mini-PEG3 linker A) and **16'** (mini-PEG3 linker B). IC_{50} values against hGOAT represent the average of three independent trials, and error bars represent one standard deviation. .

4. Conclusions

We have a demonstrated an efficient route toward creation of a customizable LC library for GOAT. This library allows for two orthogonal modes for cargo attachment, a maleimide-thiol conjugation and an azide-alkyne copper catalyzed cycloaddition. This synthesis is robust and compatible with a variety of cargo molecules differing in size and charge. These results indicate that while cargo size, flexibility, and charge can affect binding affinity to GOAT. Overall, this LC system

 doi:10.20944/preprints202412.0414.v1

can accommodate a variety of cargoes without losing potency against GOAT. These LCs will enable new studies of GOAT expression in cells and tissues and will support exploration of GOAT as a biomarker and therapeutic target.

Supplementary Materials: The following supporting information can be downloaded at the website of this paper posted on Preprints.org, Supporting synthetic methods; Analytical data for peptide ligands; Ligand-conjugate GOAT inhibitory activity; Characterization information for ligands; ^{1}H and ^{13}C NMR spectra for bifunctional adapter and synthetic intermediate

Author Contributions: Conceptualization, J.D.C. and J.L.H.; investigation, A.L.F., C.W.T, A.M.S, G.C.C., N.M., M.A.S.; formal analysis, A.L.F. and A.M.S.; resources, A.L.F. and M.A.S.; writing—original draft preparation, A.L.F. and J.L.H.; writing—review and editing, A.L.F. and J.L.H.; supervision, J.D.C. and J.L.H.; project administration, J.L.H.; funding acquisition, J.L.H. All authors have read and agreed to the published version of the manuscript.

Funding: This research was funded by the National Institutes of Health grant number GM134102 (JLH). This manuscript is also based in part upon work supported by the National Science Foundation under Grant No. CHE-1659775.

Data Availability Statement: The data and original contributions presented in this study are included in the article and supplementary material. Further inquiries can be directed to the corresponding author.

Conflicts of Interest: The authors declare no conflict of interest. The funders had no role in the design of the study; in the collection, analyses, or interpretation of data; in the writing of the manuscript; or in the decision to publish the results.

References

1. Kojima, M.; Hosoda, H.; Date, Y.; Nakazato, M.; Matsuo, H.; Kangawa, K. Ghrelin Is a Growth-Hormone-Releasing Acylated Peptide from Stomach. *Nature* **1999**, *402* (6762), 656–660. https://doi.org/10.1038/45230.
2. Cowley, M. A.; Smith, R. G.; Diano, S.; Tschöp, M.; Pronchuk, N.; Grove, K. L.; Strasburger, C. J.; Bidlingmaier, M.; Esterman, M.; Heiman, M. L.; Garcia-Segura, L. M.; Nillni, E. A.; Mendez, P.; Low, M. J.; Sotonyi, P.; Friedman, J. M.; Liu, H.; Pinto, S.; Colmers, W. F.; Cone, R. D.; Horvath, T. L. The Distribution and Mechanism of Action of Ghrelin in the CNS Demonstrates a Novel Hypothalamic Circuit Regulating Energy Homeostasis. *Neuron* **2003**, *37* (4), 649–661. https://doi.org/10.1016/S0896-6273(03)00063-1.
3. Cummings, D. E.; Frayo, R. S.; Marmonier, C.; Aubert, R.; Chapelot, D. Plasma Ghrelin Levels and Hunger Scores in Humans Initiating Meals Voluntarily without Time- and Food-Related Cues. *Am. J. Physiol.-Endocrinol. Metab.* **2004**, *287* (2), E297–E304. https://doi.org/10.1152/ajpendo.00582.2003.
4. Cummings, D. E.; Purnell, J. Q.; Frayo, R. S.; Schmidova, K.; Wisse, B. E.; Weigle, D. S. A Preprandial Rise in Plasma Ghrelin Levels Suggests a Role in Meal Initiation in Humans. *Diabetes* **2001**, *50* (8), 1714–1719. https://doi.org/10.2337/diabetes.50.8.1714.
5. Tschöp, M.; Smiley, D. L.; Heiman, M. L. Ghrelin Induces Adiposity in Rodents. *Nature* **2000**, *407* (6806), 908–913. https://doi.org/10.1038/35038090.
6. Khatib, N.; Gaidhane, S.; Gaidhane, A. M.; Khatib, M.; Simkhada, P.; Gode, D.; Zahiruddin, Q. S. Ghrelin: Ghrelin as a Regulatory Peptide in Growth Hormone Secretion. *J. Clin. Diagn. Res. JCDR* **2014**, *8* (8), MC13–MC17. https://doi.org/10.7860/JCDR/2014/9863.4767.
7. Yin, Y.; Li, Y.; Zhang, W. The Growth Hormone Secretagogue Receptor: Its Intracellular Signaling and Regulation. *Int. J. Mol. Sci.* **2014**, *15* (3), 4837–4855. https://doi.org/10.3390/ijms15034837.
8. Lutter, M.; Sakata, I.; Osborne-Lawrence, S.; Rovinsky, S. A.; Anderson, J. G.; Jung, S.; Birnbaum, S.; Yanagisawa, M.; Elmquist, J. K.; Nestler, E. J.; Zigman, J. M. The Orexigenic Hormone Ghrelin Defends against Depressive Symptoms of Chronic Stress. *Nat. Neurosci.* **2008**, *11* (7), 752–753. https://doi.org/10.1038/nn.2139.
9. Andrews, Z. B.; Erion, D.; Beiler, R.; Liu, Z.-W.; Abizaid, A.; Zigman, J.; Elsworth, J. D.; Savitt, J. M.; DiMarchi, R.; Tschöp, M.; Roth, R. H.; Gao, X.-B.; Horvath, T. L. Ghrelin Promotes and Protects Nigrostriatal Dopamine Function via a UCP2-Dependent Mitochondrial Mechanism. *J. Neurosci.* **2009**, *29* (45), 14057–14065. https://doi.org/10.1523/JNEUROSCI.3890-09.2009.
10. Meyer, R. M.; Burgos-Robles, A.; Liu, E.; Correia, S. S.; Goosens, K. A. A Ghrelin-Growth Hormone Axis Drives Stress-Induced Vulnerability to Enhanced Fear. *Mol. Psychiatry* **2014**, *19* (12), 1284–1294. https://doi.org/10.1038/mp.2013.135.
11. Harmatz, E. S.; Stone, L.; Lim, S. H.; Lee, G.; McGrath, A.; Gisabella, B.; Peng, X.; Kosoy, E.; Yao, J.; Liu, E.; Machado, N. J.; Weiner, V. S.; Slocum, W.; Cunha, R. A.; Goosens, K. A. Central Ghrelin Resistance Permits the Overconsolidation of Fear Memory. *Biol. Psychiatry* **2017**, *81* (12), 1003–1013. https://doi.org/10.1016/j.biopsych.2016.11.009.

 doi:10.20944/preprints202412.0414.v1

12. Yousufzai, M. I. ul A.; Harmatz, E. S.; Shah, M.; Malik, M. O.; Goosens, K. A. Ghrelin Is a Persistent Biomarker for Chronic Stress Exposure in Adolescent Rats and Humans. *Transl. Psychiatry* **2018**, *8*, 74. https://doi.org/10.1038/s41398-018-0135-5.
13. Soriano-Guillén, L.; Barrios, V.; Campos-Barros, A.; Argente, J. Ghrelin Levels in Obesity and Anorexia Nervosa: Effect of Weight Reduction or Recuperation. *J. Pediatr.* **2004**, *144* (1), 36–42. https://doi.org/10.1016/j.jpeds.2003.10.036.
14. Berner, L. A.; Brown, T. A.; Lavender, J. M.; Lopez, E.; Wierenga, C. E.; Kaye, W. H. Neuroendocrinology of Reward in Anorexia Nervosa and Bulimia Nervosa: Beyond Leptin and Ghrelin. *Mol. Cell. Endocrinol.* **2019**, *497*, 110320. https://doi.org/10.1016/j.mce.2018.10.018.
15. Monteleone, A. M.; Castellini, G.; Volpe, U.; Ricca, V.; Lelli, L.; Monteleone, P.; Maj, M. Neuroendocrinology and Brain Imaging of Reward in Eating Disorders: A Possible Key to the Treatment of Anorexia Nervosa and Bulimia Nervosa. *Prog. Neuropsychopharmacol. Biol. Psychiatry* **2018**, *80*, 132–142. https://doi.org/10.1016/j.pnpbp.2017.02.020.
16. Hotta, M.; Ohwada, R.; Akamizu, T.; Shibasaki, T.; Takano, K.; Kangawa, K. Ghrelin Increases Hunger and Food Intake in Patients with Restricting-Type Anorexia Nervosa: A Pilot Study. *Endocr. J.* **2009**, *56* (9), 1119–1128.
17. Fazeli, P. K.; Lawson, E. A.; Faje, A. T.; Eddy, K. T.; Lee, H.; Fiedorek, F. T.; Breggia, A.; Gaal, I. M.; DeSanti, R.; Klibanski, A. Treatment with a Ghrelin Agonist in Outpatient Women with Anorexia Nervosa: A Randomized Clinical Trial. *J. Clin. Psychiatry* **2018**, *79* (1), 17m11585. https://doi.org/10.4088/JCP.17m11585.
18. Zallar, L. J.; Farokhnia, M.; Tunstall, B. J.; Vendruscolo, L. F.; Leggio, L. Chapter Four - The Role of the Ghrelin System in Drug Addiction. In *International Review of Neurobiology*; Thiele, T. E., Ed.; The Role of Neuropeptides in Addiction and Disorders of Excessive Consumption; Academic Press, 2017; Vol. 136, pp 89–119. https://doi.org/10.1016/bs.irn.2017.08.002.
19. Leggio, L.; Ferrulli, A.; Cardone, S.; Nesci, A.; Miceli, A.; Malandrino, N.; Capristo, E.; Canestrelli, B.; Monteleone, P.; Kenna, G. A.; Swift, R. M.; Addolorato, G. Ghrelin System in Alcohol-Dependent Subjects: Role of Plasma Ghrelin Levels in Alcohol Drinking and Craving. *Addict. Biol.* **2012**, *17* (2), 452–464. https://doi.org/10.1111/j.1369-1600.2010.00308.x.
20. Koopmann, A.; Bach, P.; Schuster, R.; Bumb, J. M.; Vollstädt-Klein, S.; Reinhard, I.; Rietschel, M.; Witt, S. H.; Wiedemann, K.; Kiefer, F. Ghrelin Modulates Mesolimbic Reactivity to Alcohol Cues in Alcohol-Addicted Subjects: A Functional Imaging Study. *Addict. Biol.* **2019**, *24* (5), 1066–1076. https://doi.org/10.1111/adb.12651.
21. Farokhnia, M.; Faulkner, M. L.; Piacentino, D.; Lee, M. R.; Leggio, L. Ghrelin: From a Gut Hormone to a Potential Therapeutic Target for Alcohol Use Disorder. *Physiol. Behav.* **2019**, *204*, 49–57. https://doi.org/10.1016/j.physbeh.2019.02.008.
22. Farokhnia, M.; Portelli, J.; Lee, M. R.; McDiarmid, G. R.; Munjal, V.; Abshire, K. M.; Battista, J. T.; Browning, B. D.; Deschaine, S. L.; Akhlaghi, F.; Leggio, L. Effects of Exogenous Ghrelin Administration and Ghrelin Receptor Blockade, in Combination with Alcohol, on Peripheral Inflammatory Markers in Heavy-Drinking Individuals: Results from Two Human Laboratory Studies. *Brain Res.* **2020**, *1740*, 146851. https://doi.org/10.1016/j.brainres.2020.146851.
23. Farokhnia, M.; Abshire, K. M.; Hammer, A.; Deschaine, S. L.; Saravanakumar, A.; Cobbina, E.; You, Z.-B.; Haass-Koffler, C. L.; Lee, M. R.; Akhlaghi, F.; Leggio, L. Neuroendocrine Response to Exogenous Ghrelin Administration, Combined With Alcohol, in Heavy-Drinking Individuals: Findings From a Randomized, Double-Blind, Placebo-Controlled Human Laboratory Study. *Int. J. Neuropsychopharmacol.* **2021**, *24* (6), 464–476. https://doi.org/10.1093/ijnp/pyab004.
24. Bednarek, M. A.; Feighner, S. D.; Pong, S.-S.; McKee, K. K.; Hreniuk, D. L.; Silva, M. V.; Warren, V. A.; Howard, A. D.; Van der Ploeg, L. H. Y.; Heck, J. V. Structure−Function Studies on the New Growth Hormone-Releasing Peptide, Ghrelin: Minimal Sequence of Ghrelin Necessary for Activation of Growth Hormone Secretagogue Receptor 1a. *J. Med. Chem.* **2000**, *43* (23), 4370–4376. https://doi.org/10.1021/jm0001727.
25. Liu, H.; Sun, D.; Myasnikov, A.; Damian, M.; Baneres, J.-L.; Sun, J.; Zhang, C. Structural Basis of Human Ghrelin Receptor Signaling by Ghrelin and the Synthetic Agonist Ibutamoren. *Nat. Commun.* **2021**, *12* (1), 6410. https://doi.org/10.1038/s41467-021-26735-5.
26. Howard, A. D.; Feighner, S. D.; Cully, D. F.; Arena, J. P.; Liberator, P. A.; Rosenblum, C. I.; Hamelin, M.; Hreniuk, D. L.; Palyha, O. C.; Anderson, J.; Paress, P. S.; Diaz, C.; Chou, M.; Liu, K. K.; McKee, K. K.; Pong, S.-S.; Chaung, L.-Y.; Elbrecht, A.; Dashkevicz, M.; Heavens, R.; Rigby, M.; Sirinathsinghji, D. J. S.; Dean, D. C.; Melillo, D. G.; Patchett, A. A.; Nargund, R.; Griffin, P. R.; DeMartino, J. A.; Gupta, S. K.; Schaeffer, J. M.; Smith, R. G.; Ploeg, L. H. T. V. der. A Receptor in Pituitary and Hypothalamus That Functions in Growth Hormone Release. *Science* **1996**, *273* (5277), 974–978. https://doi.org/10.1126/science.273.5277.974
27. Kitazawa, T.; Nakamura, T.; Saeki, A.; Teraoka, H.; Hiraga, T.; Kaiya, H. Molecular Identification of Ghrelin Receptor (GHS-R1a) and Its Functional Role in the Gastrointestinal Tract of the Guinea-Pig. *Peptides* **2011**, *32* (9), 1876–1886. https://doi.org/10.1016/j.peptides.2011.07.026.

28. Shiimura, Y.; Horita, S.; Hamamoto, A.; Asada, H.; Hirata, K.; Tanaka, M.; Mori, K.; Uemura, T.; Kobayashi, T.; Iwata, S.; Kojima, M. Structure of an Antagonist-Bound Ghrelin Receptor Reveals Possible Ghrelin Recognition Mode. *Nat. Commun.* **2020**, *11* (1), 4160. https://doi.org/10.1038/s41467-020-17554-1.
29. Abizaid, A.; Hougland, J. L. Ghrelin Signaling: GOAT and GHS-R1a Take a LEAP in Complexity. *Trends Endocrinol. Metab. TEM* **2020**, *31* (2), 107–117. https://doi.org/10.1016/j.tem.2019.09.006.
30. Yang, J.; Brown, M. S.; Liang, G.; Grishin, N. V.; Goldstein, J. L. Identification of the Acyltransferase That Octanoylates Ghrelin, an Appetite-Stimulating Peptide Hormone. *Cell* **2008**, *132* (3), 387–396. https://doi.org/10.1016/j.cell.2008.01.017.
31. Gutierrez, J. A.; Solenberg, P. J.; Perkins, D. R.; Willency, J. A.; Knierman, M. D.; Jin, Z.; Witcher, D. R.; Luo, S.; Onyia, J. E.; Hale, J. E. Ghrelin Octanoylation Mediated by an Orphan Lipid Transferase. *Proc. Natl. Acad. Sci. U. S. A.* **2008**, *105* (17), 6320–6325. https://doi.org/10.1073/pnas.0800708105.
32. Darling, J. E.; Zhao, F.; Loftus, R. J.; Patton, L. M.; Gibbs, R. A.; Hougland, J. L. Structure–Activity Analysis of Human Ghrelin O-Acyltransferase Reveals Chemical Determinants of Ghrelin Selectivity and Acyl Group Recognition. *Biochemistry* **2015**, *54* (4), 1100–1110. https://doi.org/10.1021/bi5010359.
33. Lim, C. T.; Kola, B.; Grossman, A.; Korbonits, M. The Expression of Ghrelin O-Acyltransferase (GOAT) in Human Tissues. *Endocr. J.* **2011**, *58* (8), 707–710. https://doi.org/10.1507/endocrj.K11E-117.
34. Hormaechea-Agulla, D.; Gómez-Gómez, E.; Ibáñez-Costa, A.; Carrasco-Valiente, J.; Rivero-Cortés, E.; L-López, F.; Pedraza-Arevalo, S.; Valero-Rosa, J.; Sánchez-Sánchez, R.; Ortega-Salas, R.; Moreno, M. M.; Gahete, M. D.; López-Miranda, J.; Requena, M. J.; Castaño, J. P.; Luque, R. M. Ghrelin O-Acyltransferase (GOAT) Enzyme Is Overexpressed in Prostate Cancer, and Its Levels Are Associated with Patient's Metabolic Status: Potential Value as a Non-Invasive Biomarker. *Cancer Lett.* **2016**, *383* (1), 125–134. https://doi.org/10.1016/j.canlet.2016.09.022.
35. Jiménez-Vacas, J. M.; Gómez-Gómez, E.; Montero-Hidalgo, A. J.; Herrero-Aguayo, V.; L-López, F.; Sánchez-Sánchez, R.; Guler, I.; Blanca, A.; Méndez-Vidal, M. J.; Carrasco, J.; Lopez-Miranda, J.; Requena-Tapia, M. J.; Castaño, J. P.; Gahete, M. D.; Luque, R. M. Clinical Utility of Ghrelin-O-Acyltransferase (GOAT) Enzyme as a Diagnostic Tool and Potential Therapeutic Target in Prostate Cancer. *J. Clin. Med.* **2019**, *8* (12), 2056. https://doi.org/10.3390/jcm8122056.
36. Gómez-Gómez, E.; Jiménez-Vacas, J. M.; Carrasco-Valiente, J.; Herrero-Aguayo, V.; Blanca-Pedregosa, A. M.; León-González, A. J.; Valero-Rosa, J.; Fernández-Rueda, J. L.; González-Serrano, T.; López-Miranda, J.; Gahete, M. D.; Castaño, J. P.; Requena-Tapia, M. J.; Luque, R. M. Plasma Ghrelin O-acyltransferase (GOAT) Enzyme Levels: A Novel Non-invasive Diagnosis Tool for Patients with Significant Prostate Cancer. *J. Cell. Mol. Med.* **2018**, *22* (11), 5688–5697. https://doi.org/10.1111/jcmm.13845.
37. Gahete, M. D.; Córdoba-Chaćon, J.; Hergueta-Redondo, M.; Martińez-Fuentes, A. J.; Kineman, R. D.; Moreno Bueno, G.; Luque, R. M.; Castaño, J. P. A Novel Human Ghrelin Variant (In1-Ghrelin) and Ghrelin-O-Acyltransferase Are Overexpressed in Breast Cancer: Potential Pathophysiological Relevance. **2011**. https://doi.org/10.1371/journal.pone.0023302.
38. Seim, I.; Jeffery, P. L.; de Amorim, L.; Walpole, C. M.; Fung, J.; Whiteside, E. J.; Lourie, R.; Herington, A. C.; Chopin, L. K. Ghrelin O-Acyltransferase (GOAT) Is Expressed in Prostate Cancer Tissues and Cell Lines and Expression Is Differentially Regulated in Vitro by Ghrelin. *Reprod. Biol. Endocrinol. RBE* **2013**, *11*, 70. https://doi.org/10.1186/1477-7827-11-70.
39. Jeffery, P. L.; Murray, R. E.; Yeh, A. H.; McNamara, J. F.; Duncan, R. P.; Francis, G. D.; Herington, A. C.; Chopin, L. K. Expression and Function of the Ghrelin Axis, Including a Novel Preproghrelin Isoform, in Human Breast Cancer Tissues and Cell Lines. **2005**. https://doi.org/10.1677/erc.1.00984.
40. Yeh, A. H.; Jeffery, P. L.; Duncan, R. P.; Herington, A. C.; Chopin, L. K. Ghrelin and a Novel Preproghrelin Isoform Are Highly Expressed in Prostate Cancer and Ghrelin Activates Mitogen-Activated Protein Kinase in Prostate Cancer. *Clin. Cancer Res. Off. J. Am. Assoc. Cancer Res.* **2005**, *11* (23), 8295–8303. https://doi.org/10.1158/1078-0432.CCR-05-0443.
41. Cassoni, P.; Ghé, C.; Marrocco, T.; Tarabra, E.; Allia, E.; Catapano, F.; Deghenghi, R.; Ghigo, E.; Papotti, M.; Muccioli, G. Expression of Ghrelin and Biological Activity of Specific Receptors for Ghrelin and Des-Acyl Ghrelin in Human Prostate Neoplasms and Related Cell Lines. *Eur. J. Endocrinol.* **2004**, *150* (2), 173–184. https://doi.org/10.1530/eje.0.1500173.
42. Jeffery, P. L.; Herington, A. C.; Chopin, L. K. Expression and Action of the Growth Hormone Releasing Peptide Ghrelin and Its Receptor in Prostate Cancer Cell Lines. *J. Endocrinol.* **2002**, *172* (3), R7-11. https://doi.org/10.1677/joe.0.172r007.
43. Hormaechea-Agulla, D.; Gahete, M. D.; Jiménez-Vacas, J. M.; Gómez-Gómez, E.; Ibáñez-Costa, A.; L-López, F.; Rivero-Cortés, E.; Sarmento-Cabral, A.; Valero-Rosa, J.; Carrasco-Valiente, J.; Sánchez-Sánchez, R.; Ortega-Salas, R.; Moreno, M. M.; Tsomaia, N.; Swanson, S. M.; Culler, M. D.; Requena, M. J.; Castaño, J. P.; Luque, R. M. The Oncogenic Role of the In1-Ghrelin Splicing Variant in Prostate Cancer Aggressiveness. *Mol. Cancer* **2017**, *16*, 146. https://doi.org/10.1186/s12943-017-0713-9.
44. Campaña, M. B.; Davis, T. R.; Novak, S. X.; Cleverdon, E. R.; Bates, M.; Krishnan, N.; Curtis, E. R.; Childs, M. D.; Pierce, M. R.; Morales-Rodriguez, Y.; Sieburg, M. A.; Hehnly, H.; Luyt, L. G.; Hougland, J. L. Cellular

 doi:10.20944/preprints202412.0414.v1

Uptake of a Fluorescent Ligand Reveals Ghrelin O-Acyltransferase Interacts with Extracellular Peptides and Exhibits Unexpected Localization for a Secretory Pathway Enzyme. *ACS Chem. Biol.* **2023**, *18* (8), 1880–1890. https://doi.org/10.1021/acschembio.3c00334.

45. Kearns, J. T.; Lin, D. W. Improving the Specificity of PSA Screening with Serum and Urine Markers. *Curr. Urol. Rep.* **2018**, *19* (10), 80. https://doi.org/10.1007/s11934-018-0828-6.
46. Campaña, M. B.; Irudayanathan, F. J.; Davis, T. R.; McGovern-Gooch, K. R.; Loftus, R.; Ashkar, M.; Escoffery, N.; Navarro, M.; Sieburg, M. A.; Nangia, S.; Hougland, J. L. The Ghrelin O-Acyltransferase Structure Reveals a Catalytic Channel for Transmembrane Hormone Acylation. *J. Biol. Chem.* **2019**, *294* (39), 14166–14174. https://doi.org/10.1074/jbc.AC119.009749.
47. Minciacchi, V. R.; Zijlstra, A.; Rubin, M. A.; Di Vizio, D. Extracellular Vesicles for Liquid Biopsy in Prostate Cancer: Where Are We and Where Are We Headed? *Prostate Cancer Prostatic Dis.* **2017**, *20* (3), 251–258. https://doi.org/10.1038/pcan.2017.7.
48. Dong, L.; Zieren, R. C.; Wang, Y.; de Reijke, T. M.; Xue, W.; Pienta, K. J. Recent Advances in Extracellular Vesicle Research for Urological Cancers: From Technology to Application. *Biochim. Biophys. Acta BBA - Rev. Cancer* **2019**, *1871* (2), 342–360. https://doi.org/10.1016/j.bbcan.2019.01.008.
49. Cleverdon, E. R.; Davis, T. R.; Hougland, J. L. Functional Group and Stereochemical Requirements for Substrate Binding by Ghrelin O-Acyltransferase Revealed by Unnatural Amino Acid Incorporation. *Bioorganic Chem.* **2018**, *79*, 98–106. https://doi.org/10.1016/j.bioorg.2018.04.009.
50. Millennium Pharmaceuticals, Inc. *A Phase 1/2 Dose Escalation Trial of Multiple Doses of MLN2704 (DM1 Conjugated Monoclonal Antibody MLN591) in Subjects With Metastatic Androgen-Independent Prostate Cancer*; Clinical trial registration NCT00070837; clinicaltrials.gov, 2007. https://clinicaltrials.gov/study/NCT00070837 (accessed 2024-11-04).
51. Ambrx, Inc. *A Phase 1, Multicenter, Open-Label, Dose-Escalation, and Dose-Expansion Study to Evaluate the Safety, Pharmacokinetics, and Anti-Tumor Activity of ARX517 in Subjects With Metastatic Castration-Resistant Prostate Cancer Who Are Resistant or Refractory to Prior Standard Therapies*; Clinical trial registration NCT04662580; clinicaltrials.gov, 2024. https://clinicaltrials.gov/study/NCT04662580 (accessed 2024-11-04).
52. Flavell, R. *A First-in-Human, Pilot PET Imaging Study of 89Zr-DFO-YS5, an immunoPET Agent for Detecting CD46 Positive Malignancy in Men With Prostate Cancer*; Clinical trial registration NCT05245006; clinicaltrials.gov, 2024. https://clinicaltrials.gov/study/NCT05245006 (accessed 2024-11-04).
53. Aggarwal, R. *A Phase 1b/2 Study of FOR46 in Combination With Enzalutamide in Patients With Metastatic Castration Resistant Prostate Cancer*; Clinical trial registration NCT05011188; clinicaltrials.gov, 2024. https://clinicaltrials.gov/study/NCT05011188 (accessed 2024-11-04).
54. Fu, Z.; Li, S.; Han, S.; Shi, C.; Zhang, Y. Antibody Drug Conjugate: The "Biological Missile" for Targeted Cancer Therapy. *Signal Transduct. Target. Ther.* **2022**, *7* (1), 1–25. https://doi.org/10.1038/s41392-022-00947-7.
55. Tagawa, S. T.; Beltran, H.; Vallabhajosula, S.; Goldsmith, S. J.; Osborne, J.; Matulich, D.; Petrillo, K.; Parmar, S.; Nanus, D. M.; Bander, N. H. Anti-Prostate Specific Membrane Antigen-Based Radioimmunotherapy for Prostate Cancer. *Cancer* **2010**, *116* (4 Suppl), 1075–1083. https://doi.org/10.1002/cncr.24795.
56. Elsässer-Beile, U.; Reischl, G.; Wiehr, S.; Bühler, P.; Wolf, P.; Alt, K.; Shively, J.; Judenhofer, M. S.; Machulla, H.-J.; Pichler, B. J. PET Imaging of Prostate Cancer Xenografts with a Highly Specific Antibody against the Prostate-Specific Membrane Antigen. *J. Nucl. Med.* **2009**, *50* (4), 606–611. https://doi.org/10.2967/jnumed.108.058487.
57. Mjaess, G.; Aoun, F.; Rassy, E.; Diamand, R.; Albisinni, S.; Roumeguère, T. Antibody-Drug Conjugates in Prostate Cancer: Where Are We? *Clin. Genitourin. Cancer* **2023**, *21* (1), 171–174. https://doi.org/10.1016/j.clgc.2022.07.009.
58. Sardinha, M.; Palma dos Reis, A. F.; Barreira, J. V.; Fontes Sousa, M.; Pacey, S.; Luz, R. Antibody-Drug Conjugates in Prostate Cancer: A Systematic Review. *Cureus 15* (2), e34490. https://doi.org/10.7759/cureus.34490.
59. Pierce, M. R.; Hougland, J. L. A Rising Tide Lifts All MBOATs: Recent Progress in Structural and Functional Understanding of Membrane Bound O-Acyltransferases. *Front. Physiol.* **2023**, *14*. https://doi.org/10.3389/fphys.2023.1167873.
60. Liu, Y.; Qi, X.; Donnelly, L.; Elghobashi-Meinhardt, N.; Long, T.; Zhou, R. W.; Sun, Y.; Wang, B.; Li, X. Mechanisms and Inhibition of Porcupine-Mediated Wnt Acylation. *Nature* **2022**, *607* (7920), 816. https://doi.org/10.1038/s41586-022-04952-2.
61. Coupland, C. E.; Andrei, S. A.; Ansell, T. B.; Carrique, L.; Kumar, P.; Sefer, L.; Schwab, R. A.; Byrne, E. F.; Pardon, E.; Steyaert, J.; Magee, A. I.; Lanyon-Hogg, T.; Sansom, M. S.; Tate, E. W.; Siebold, C. Structure, Mechanism, and Inhibition of Hedgehog Acyltransferase. *Mol. Cell* **2021**, *81* (24), 5025. https://doi.org/10.1016/j.molcel.2021.11.018.
62. Jiang, Y.; Benz, T. L.; Long, S. B. Substrate and Product Complexes Reveal Mechanisms of Hedgehog Acylation by HHAT. *Science* **2021**, *372* (6547), 1215. https://doi.org/10.1126/science.abg4998.

 doi:10.20944/preprints202412.0414.v1

63. Ainavarapu, S. R. K.; Brujić, J.; Huang, H. H.; Wiita, A. P.; Lu, H.; Li, L.; Walther, K. A.; Carrion-Vazquez, M.; Li, H.; Fernandez, J. M. Contour Length and Refolding Rate of a Small Protein Controlled by Engineered Disulfide Bonds. *Biophys. J.* **2006**, *92* (1), 225. https://doi.org/10.1529/biophysj.106.091561.
64. Chakraborty, S.; Venkatramani, R.; Rao, B. J.; Asgeirsson, B.; Dandekar, A. M. Protein Structure Quality Assessment Based on the Distance Profiles of Consecutive Backbone Cα Atoms. *F1000Research* **2013**, *2*, 211. https://doi.org/10.12688/f1000research.2-211.v3.
65. Rassy, E.; Rached, L.; Pistilli, B. Antibody Drug Conjugates Targeting HER2: Clinical Development in Metastatic Breast Cancer. *The Breast* **2022**, *66*, 217–226. https://doi.org/10.1016/j.breast.2022.10.016.
66. Darling, J. E.; Prybolsky, E. P.; Sieburg, M.; Hougland, J. L. A Fluorescent Peptide Substrate Facilitates Investigation of Ghrelin Recognition and Acylation by Ghrelin *O*-Acyltransferase. *Anal. Biochem.* **2013**, *437* (1), 68–76.
67. Sieburg, M. A.; Cleverdon, E. R.; Hougland, J. L. Biochemical Assays for Ghrelin Acylation and Inhibition of Ghrelin O-Acyltransferase. In *Protein Lipidation: Methods and Protocols*; Linder, M. E., Ed.; Methods in Molecular Biology; Springer: New York, NY, 2019; pp 227–241. https://doi.org/10.1007/978-1-4939-9532-5_18.
68. Lewis Phillips, G. D.; Li, G.; Dugger, D. L.; Crocker, L. M.; Parsons, K. L.; Mai, E.; Blättler, W. A.; Lambert, J. M.; Chari, R. V. J.; Lutz, R. J.; Wong, W. L. T.; Jacobson, F. S.; Koeppen, H.; Schwall, R. H.; Kenkare-Mitra, S. R.; Spencer, S. D.; Sliwkowski, M. X. Targeting HER2-Positive Breast Cancer with Trastuzumab-DM1, an Antibody–Cytotoxic Drug Conjugate. *Cancer Res.* **2008**, *68* (22), 9280–9290. https://doi.org/10.1158/0008-5472.CAN-08-1776.
69. Fernandez, R. M.; Ito, A. S.; Schiöth, H. B.; Lamy, M. T. Structural Study of Melanocortin Peptides by Fluorescence Spectroscopy: Identification of β-(2-Naphthyl)-d-Alanine as a Fluorescent Probe. *Biochim. Biophys. Acta BBA - Gen. Subj.* **2003**, *1623* (1), 13–20. https://doi.org/10.1016/S0304-4165(03)00152-1.
70. Tinsley, I. C.; Borner, T.; Swanson, M. L.; Chepurny, O. G.; Doebley, S. A.; Kamat, V.; Sweet, I. R.; Holz, G. G.; Hayes, M. R.; De Jonghe, B. C.; Doyle, R. P. Synthesis, Optimization, and Biological Evaluation of Corrinated Conjugates of the GLP-1R Agonist Exendin-4. *J. Med. Chem.* **2021**, *64* (6), 3479–3492. https://doi.org/10.1021/acs.jmedchem.1c00185.
71. Hong, V.; Presolski, S. I.; Ma, C.; Finn, M. G. Analysis and Optimization of Copper-Catalyzed Azide–Alkyne Cycloaddition for Bioconjugation. *Angew. Chem. Int. Ed.* **2009**, *48* (52), 9879–9883. https://doi.org/10.1002/anie.200905087.